The numerical simulation for foamy oil flow in porous media

T. Ko[1], D.D. Joseph[1], R. Bai[1] and A.M. Kamp[2]

[1] Univ. of Minnesota, Dept. of Aerospace Engng. & Mech., 107 Akerman Hall
110 Union St. S.E., Minneapolis, MN 55455, USA
[2] PDVSA Intevep, PO Box 76343, Caracas 1070-A, Venezuela

September 12, 2001

1. Constitutive equations relating the dispersed gas fraction to the pressure

The time derivatives have a material derivative

$$\frac{D}{Dt} = \alpha \frac{\partial}{\partial t} + \mathbf{u} \cdot \nabla \tag{1-1}$$

where α is the porosity. The constitutive equations are written as follows;

$$\tau_1 \frac{D}{Dt}\left(\frac{\phi}{1-\phi}\right) + \tau_2 \frac{D}{Dt}\left(\frac{\tilde{p}-p}{p}\right) = \frac{\tilde{p}-p}{p} - \frac{\beta\phi}{1-\phi}. \tag{1-2}$$

$$\alpha \frac{\partial \phi}{\partial t} + u \cdot \nabla \phi - (1-\phi)\operatorname{div} \mathbf{u} = 0. \tag{1-3}$$

$$\mathbf{u} = -\lambda \nabla p. \tag{1-4}$$

2. Dimensionless equations and governing parameters for one dimensional problem

We introduce dimensionless variables as follows;

$$X = x / L,$$
$$T = t / \Theta$$
$$\Lambda(\Psi) = \lambda(\phi)/\lambda_0 = \left(\frac{1}{1+\Psi}\right)^m$$
$$J_1 = \tau_1 \tilde{p} \lambda_0 / L^2$$
$$J_1 = \tau_{21} \tilde{p} \lambda_0 / L^2$$

$$\mathbf{\Psi} = \frac{\phi}{1-\phi}$$
$$\mathbf{P} = \frac{1-P}{P} = \frac{\tilde{p}-p}{p} \tag{2-1}$$
$$\mathbf{U} = \frac{\mathbf{u}\,L}{\lambda_0 \tilde{p}}$$

and find that if

$$\mathbf{\Theta} = \alpha L^2 / \lambda_0 \tilde{p}\,. \tag{2-2}$$

Then, we can write equations (1-2), (1-3) and (1-4) as follows;

$$J_1\left\{\frac{\partial \mathbf{\Psi}}{\partial T} + \mathbf{U}\frac{\partial \mathbf{\Psi}}{\partial X}\right\} + J_2\left\{\frac{\partial \mathbf{P}}{\partial T} + \mathbf{U}\frac{\partial \mathbf{P}}{\partial X}\right\} = \mathbf{P} - \beta\mathbf{\Psi} \tag{2-3}$$

$$\frac{1}{1+\mathbf{\Psi}}\left\{\frac{\partial \mathbf{\Psi}}{\partial T} + \mathbf{U}\frac{\partial \mathbf{\Psi}}{\partial X}\right\} = \frac{\partial \mathbf{U}}{\partial X} \tag{2-4}$$

$$\mathbf{U} = \mathbf{\Lambda}\frac{1}{(\mathbf{P}+1)^2}\frac{\partial \mathbf{P}}{\partial X} = \frac{\left(\frac{1}{1+\mathbf{\Psi}}\right)^m}{(\mathbf{P}+1)^2}\frac{\partial \mathbf{P}}{\partial X}\,. \tag{2-5}$$

3. Numerical method

To solve the fully implicit constitutive equations, We write again them as follows;

$$\mathbf{U}' = \left\{\left(\frac{1}{1+\mathbf{\Psi}^{n-1}}\right)^m \Big/ \left(\mathbf{P}^{n-1}+1\right)^2\right\}\frac{\partial \mathbf{P}^{n-1}}{\partial X} \tag{2-6}$$

$$\frac{1}{1+\mathbf{\Psi}^*}\frac{\mathbf{\Psi}^n - \mathbf{\Psi}^{n-1}}{\Delta T} + \frac{1}{2}\mathbf{U}'\left\{\frac{\partial \mathbf{\Psi}^n}{\partial X} + \frac{\partial \mathbf{\Psi}^{n-1}}{\partial X}\right\} = \frac{\partial \mathbf{U}'}{\partial X} \tag{2-7}$$

$$\mathbf{U}'' = \left\{\left(\frac{1}{1+\mathbf{\Psi}^{n}}\right)^m \Big/ \left(\mathbf{P}^{n-1}+1\right)^2\right\}\frac{\partial \mathbf{P}^{n-1}}{\partial X} \tag{2-8}$$

$$J_2 \frac{\mathbf{P}^n - \mathbf{P}^{n-1}}{\Delta T} + \frac{1}{2} J_2 \mathbf{U}^n \left\{ \frac{\partial \mathbf{P}^n}{\partial X} + \frac{\partial \mathbf{P}^{n-1}}{\partial X} \right\} - \frac{1}{2} \left(\mathbf{P}^n + \mathbf{P}^{n-1} \right)$$
$$= -J_1 \left\{ \frac{\boldsymbol{\Psi}^n - \boldsymbol{\Psi}^{n-1}}{\Delta T} + \mathbf{U}^n \frac{\partial \boldsymbol{\Psi}^n}{\partial X} \right\} - \beta \boldsymbol{\Psi}^n \qquad (2\text{-}9)$$

where the superscript n indicates the time level and **U**' is intermediate velocity. Before solving Eq. (2-7), velocity is updated with the values at previous time step through Eq.(2-6). The velocity is calculated again with the new value of $\boldsymbol{\Psi}$ obtained from Eq. (2-8) and used in Eq. (2-9) to calculate **P** with updated value of $\boldsymbol{\Psi}$. By calculating Eq. (2-5) two times, we can get converged value for each time step more quickly.

The constitutive equations are discretized using a Galerkin method. The weak formulations of the constitutive equation are derived by multiply them by a corresponding weighting function and integrating over the spatial domain of a problem. On Eq. (2-7), the $\boldsymbol{\Psi}^*$ is used to linearize the continuity equation. The main iteration is the loop of calculation for four-step equations (2-6), (2-7), (2-8) and (2-9) to get the converged value of variables **U**, **P** and $\boldsymbol{\Psi}$ at each time step. The converged value for $\boldsymbol{\Psi}^*$ is obtained by iterating the Eq. (2-6) in each main iteration.

4. Numerical result

In order to find the best fitting parameters J_1, J_2 and m to fit the experiments of Maini and Sarma, we tried several cases for various values of three parameters by solving the three constitutive equations with the method described on the previous section. The pressure profile and accumulating oil production at outlet is obtained from the both steady and unsteady simulation for various J_1, J_2 and m. The results are compared with

the experiments data. Through our simulation, the parameters which give a best fit to experiments data are obtained as J_1 = 200, J_2 = -18 and m = 9.

The following figures 4-1 and 4-2 shows the comparison of the numerical result for J_1 = 200, J_2 = -18 and m = 9 with the experiments result for steady state. The boundary conditions for steady problem are given as follows;

$$P = 1 \quad , \phi = 0 \qquad \text{at } X = 0$$

$$P = p_L / \tilde{p} \qquad \text{at } X = 1$$

where p_L is outlet pressure and $\tilde{p}$ is saturation pressure.

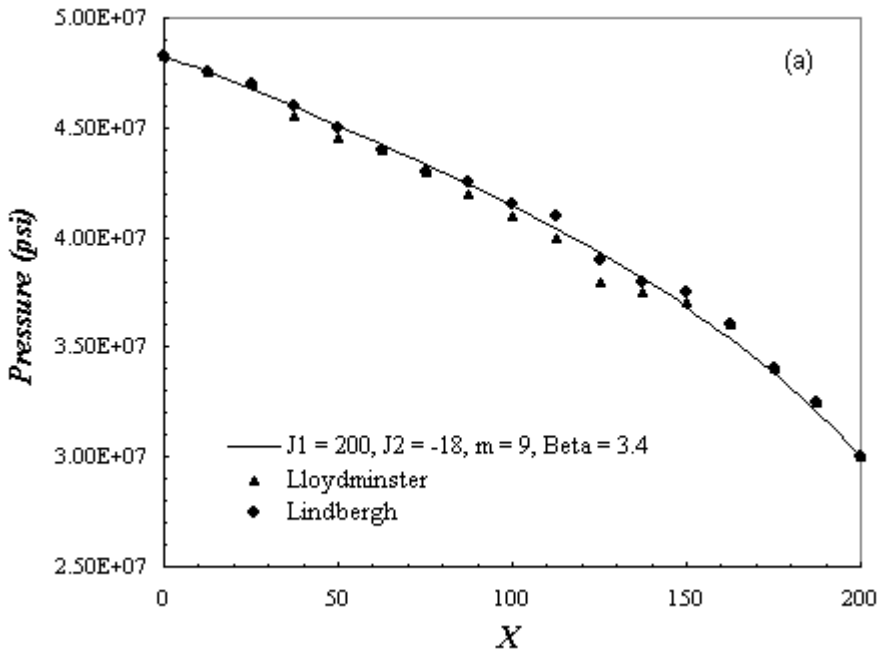

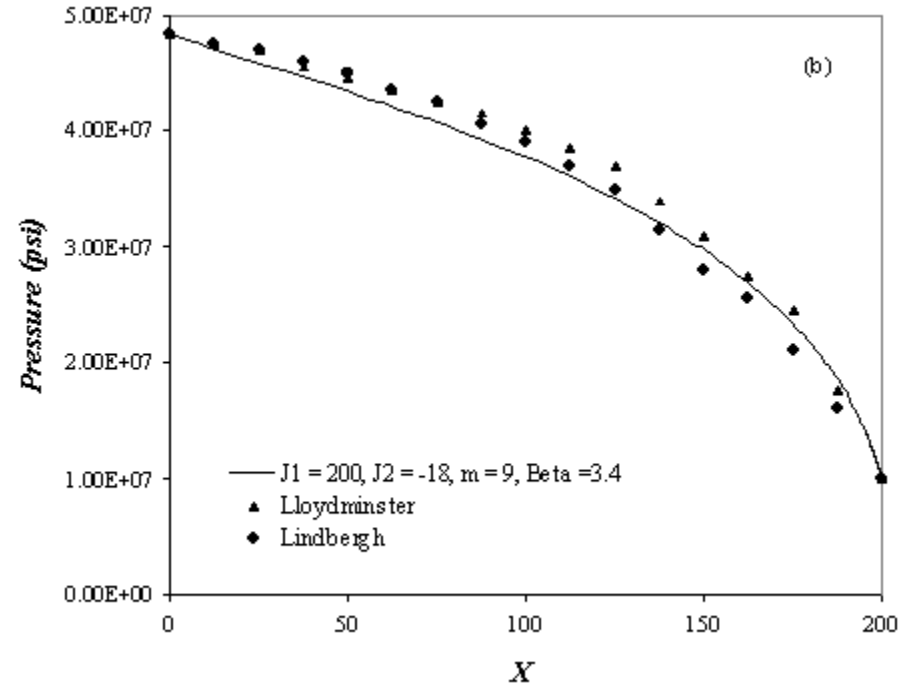

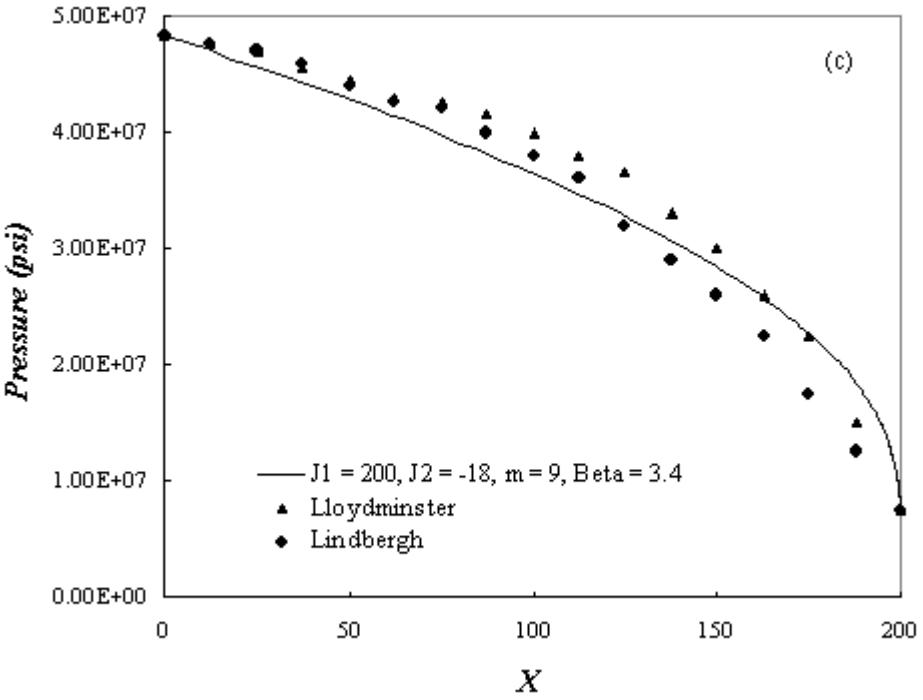

Figure 4-1. Comparison of numerical and experimental pressure distribution at various drawdown pressure. (a) is for p_L = 30Mpsi, (b) is for p_L = 10Mpsi and (c) is for p_L = 7.5Mpsi.

Figure 4-1 shows the numerical pressure distribution for J_1 = 200, J_2 = -18 and m = 9 and experimental one at drawdown pressure p_L = 30, 10 and 7.5Mpsi. Figure 4-2 shows the numerical oil production rate in steady flow for J_1 = 200, J_2 = -18, m = 9 and β = 3.4 at various drawdown pressures $p_L - \tilde{p}$.

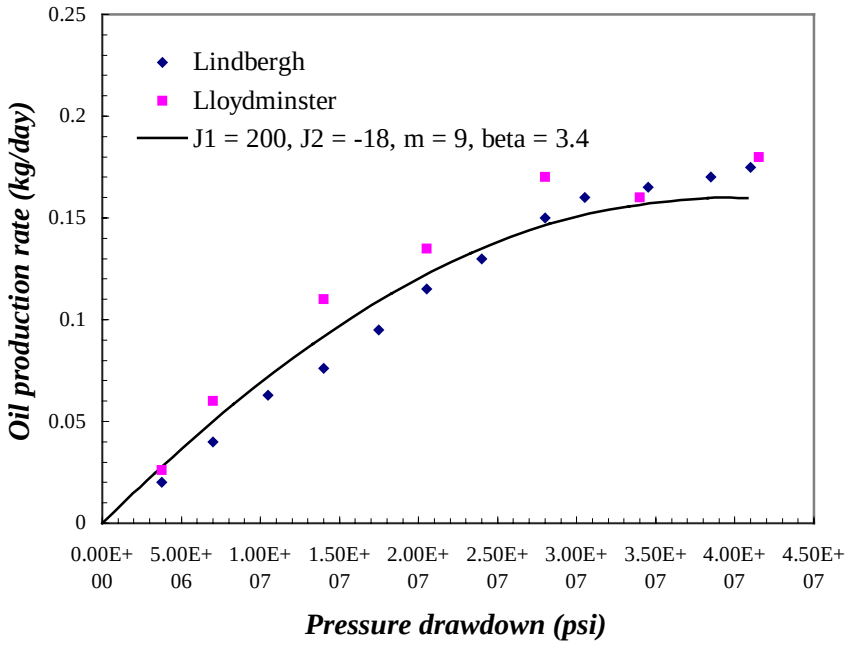

Figure 4-2. Comparison of numerical and experimental oil production rates at various pressure drawdowns.

The boundary conditions and initial conditions for unsteady flows are given as follows;

$$P = 1, \quad \phi = 0 \quad \text{for } 0 \le X \le 1 \quad \text{when } T = 0$$

$$\frac{\partial P}{\partial X} = 0 \qquad \text{at X = 0}$$

$$P = p_L / \tilde{p} \qquad \text{at X = 1}$$

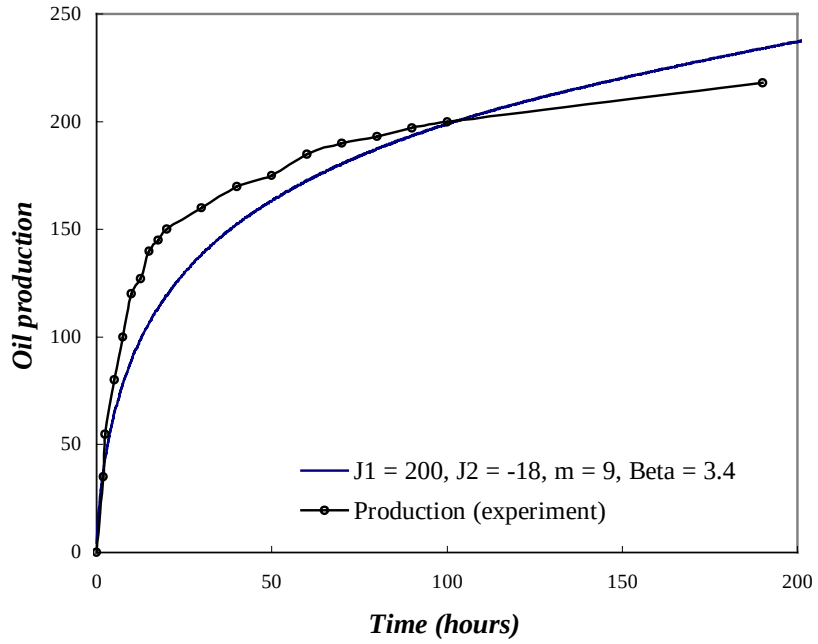

Figure 4-3. Comparison of numerical and experimental accumulating oil production for unsteady flow.

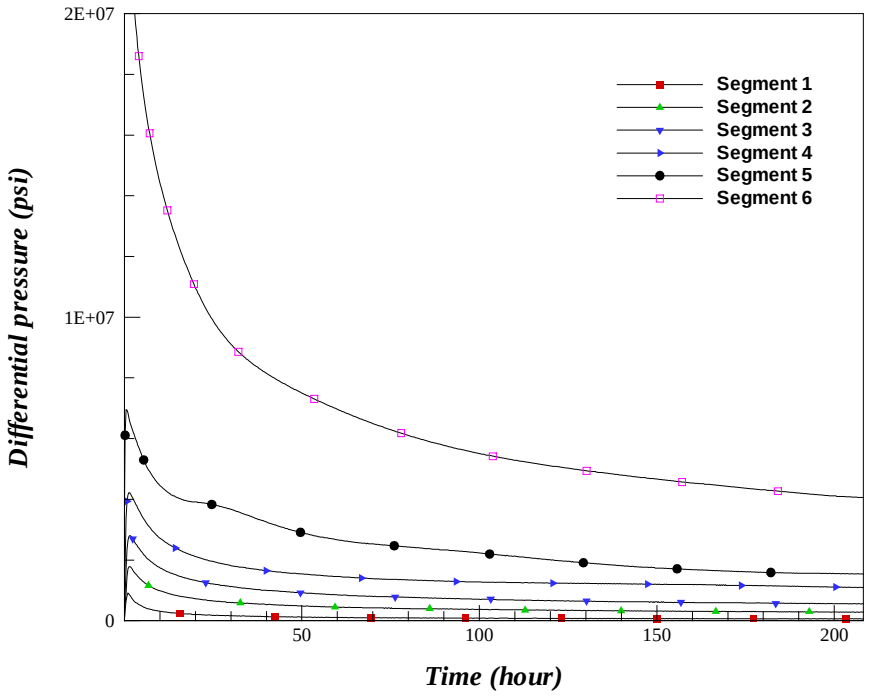

Figure 4-4. The numerical differential pressure in 6 segments at J_1 = 200, J_2 = -18, m = 9 and β = 3.4 for the blowdown problem.

The numerical and experimental cumulative oil productions for unsteady flows are shown in figure 4-3.The numerical result and experiments data of differential pressure in 6 segments defined by pressure taps is given in figure 4-4 and 4-5, respectively. The numerical result for steady flows is comparatively close to experiments. Even if the numerical results for unsteady flows do not give good fitting to experiments, the parameters J_1 = 200, J_2 = -18 and m = 9 offers the best fit for both of cases.

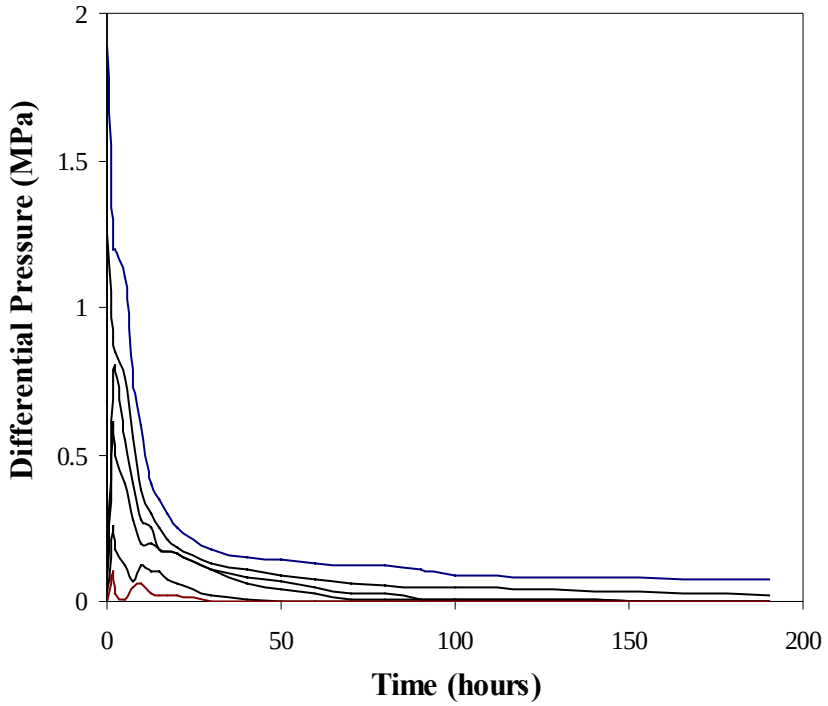

Figure 4.5: (Maini & Sarma, 1994). Change in the pressure drop across different core segments with time during the blowdown experiment with the Lloydminster system.

Figure 4.6 shows the numerical result of average pressure for the various depletion rates. For the numerical calculation, we used the same values for all parameter as in Kumar, Pooladi-Darvish and Okazawa (2000). The initial pressure 620psi is higher than the bubble point pressure of oil 575psi. We can not obtain the pressure overshoot observed in depletion experiments performed on sand packs. Figure 4.7 shows the average pressure vs. depletion for our numerical result and experimental and simulated

data in Kumar (2000). The initial pressure is used as the bubble point pressure of oil 575psi

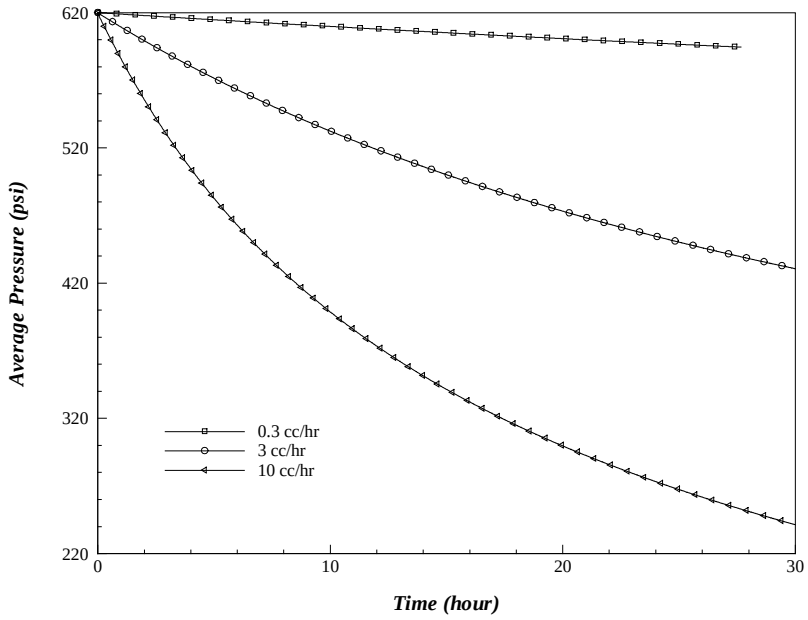

Figure 4.6. The average pressure vs. time for the various depletion rates of 0.3cc/hr, 3cc/hr and 10cc/hr.

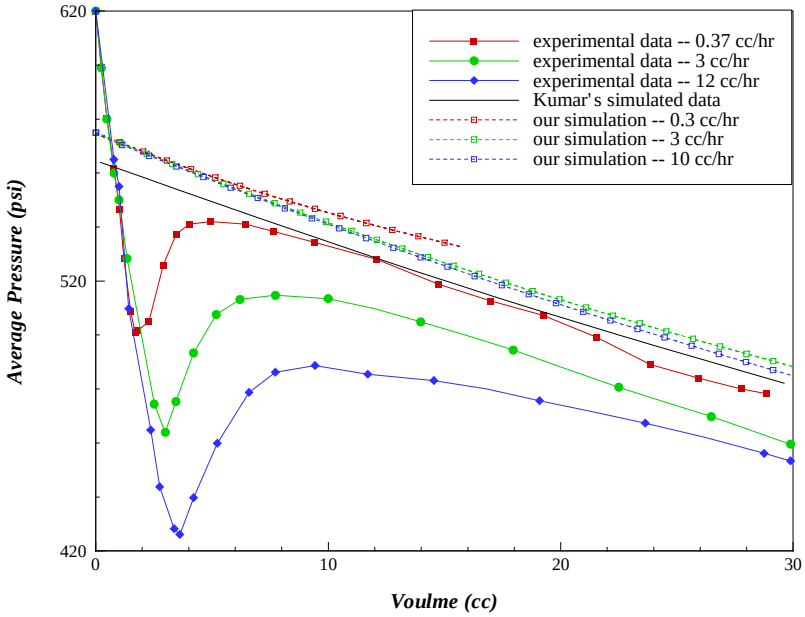

Figure 4.7. Comparison of the numerical and experimental data for average pressure vs. depletion.